Water Resources Management (2026) 40:285
https://doi.org/10.1007/s11269-026-04637-9

Scaling Approaches for Manning's Roughness Coefficient in Reduced-Scale Hydrodynamic River Simulations With Delft3D

Amira S. Farag[1] · **Mohamed B. Ezzat**[1] · **M. M. Ibrahim**[2]

Received: 5 December 2025 / Accepted: 31 March 2026

Abstract
Despite extensive theoretical work on Manning's roughness coefficient (n) in hydraulic literature, its numerical validity across multiple scales in two-dimensional depth-averaged (2DH) frameworks remains poorly quantified. This study addresses this gap by developing a systematic multi-scale calibration protocol applied to a complex reach of a large alluvial river. The novelty lies in the simultaneous evaluation of three geometric ratios (1:10, 1:20, and 1:30) within a single modeling environment to derive an empirically grounded scaling relationship. Results demonstrate that prototype roughness is not directly transferable: unscaled parameters yield errors 25 to 50 times greater than optimal configurations. A nonlinear power-law relationship is identified between the scale ratio and the required roughness reduction, achieving 98% mean agreement with classical Froude–Manning theory. Crucially, this research identifies the 1:20 scale as the optimal threshold for minimizing scale-induced numerical distortions. By quantifying the slight deviation from theoretical exponents caused by the numerical "absorption" of three-dimensional turbulent structures into two-dimensional parameters, this work provides a physics-based predictive tool that eliminates subjective trial-and-error calibration in downscaled river simulations.

Keywords Manning's roughness coefficient · Scale effects · Delft3D · Hydrodynamic modeling · Froude similarity · River downscaling · Empirical equation

✉ Amira S. Farag
amira.ghazala@yahoo.com

[1] Hydraulic Research Institute HRI, National Water Research Center NWRC, Ministry of Water Resources and Irrigation MWRI, Giza 13621, Egypt

[2] Irrigation and Hydraulics Dept., Shoubra Faculty of Engineering, Benha University, Cairo, Egypt

Published online: 05 May 2026

1 Introduction

Accurate hydrodynamic modeling underpins effective flood risk assessment, water resource management, and aquatic habitat restoration (Kant et al. 2025; Yang et al. 2021). Numerical modeling has advanced from 1D to sophisticated 2DH frameworks in large-scale applications (Bates et al. 2021; Teng et al. 2017). As models simulate extreme floods and complex sediment dynamics, balancing accuracy and efficiency has become critical (Horritt and Bates 2002; Neal et al. 2012). Consequently, modern 2DH models must account for secondary currents and localized turbulence previously overlooked (Lazzarin and Viero 2022; Dottori et al. 2013). This evolution necessitates re-evaluating modeling assumptions, notably empirical parameter selection and scaling. Downscaling hydraulic models provides essential insights but introduces scale effects that degrade performance. Dimensional analysis reduces complex relationships to dimensionless groups. In compound channels, dimensional analysis successfully predicts zonal flow distribution (Devi et al. 2025). Froude similarity enforces inertia–gravity balance, giving partial dynamic similarity. However, full similarity requires controlling viscous, surface-tension, and compressibility effects that Froude matching alone cannot provide, especially in small-scale or highly turbulent systems (Tartandyo et al. 2024). In turbulent free-surface flows, simultaneously satisfying Froude and Reynolds similarity is impossible, distorting viscous and roughness-related processes (Heller 2011). In recirculating flows, Froude-scale effects weaken vortices and increase energy losses (Tartandyo et al. 2024). Similarly, wave energy converters show that Froude scaling alone does not capture viscous and inertial effects (Windt et al. 2021). While Manning's n is theoretically expected to scale as $nr = Lr^{1/6}$, this relationship lacks systematic multi-scale validation. Flow resistance power-laws link to the turbulent energy cascade, requiring scaling laws to account for eddy–bed interactions (Gioia and Bombardelli 2001). Accurately determining Manning's *n* remains a central challenge (Chow 1959). Traditional calibration relies on manual trial-and-error (Hameed 2013), a labor-intensive, subjective approach (Boulomytis et al. 2017). Sensitivity techniques like elementary effects guide calibration (Morris 2018; Campolongo et al. 2007). Automated frameworks, such as Particle Swarm Optimization, enable efficient calibration with uncertainty quantification (Shahverdi and Talebmorad 2023). Global sensitivity methods assess parameter importance in hydraulic models (Saltelli et al. 2019). Hybrid approaches integrating physical laws with empirical data show promise. Haroun et al. (2025) used a semi-theoretical framework based on Euler's equations and Froude number to evaluate bed roughness effects on hydraulic jumps. Rad et al. (2025) combined image processing with machine learning to estimate Manning's n dynamically, achieving near-perfect classification (99%). Yuan and Lozano-Durán (2025) introduced IT-π, an information-theoretic framework for discovering optimal dimensionless variables, showing predictive capability is limited by information shared between inputs and outputs—a principle informing scaling parameter selection. Despite these advances, absorbing unresolved 3D flow structures into 2D empirical parameters remains a critical gap (Lazzarin and Viero 2022). Zafar and Phanikumar (2026) show roughness parameters may not transfer across flood regimes, underscoring the need for robust scaling relationships—a challenge this study directly addresses.

1.1 Novelty and Objectives

The novelty of this study lies in systematically bridging the gap between theoretical roughness power laws and actual numerical performance. This is achieved through a multi-scale evaluation of Manning's n at three geometric ratios (1:10, 1:20, and 1:30) within a single modeling framework. Using the Delft3D-FLOW system (Deltares 2022), the study establishes an empirically grounded calibration protocol for downscaled river models.

The primary objective is to test a streamlined downscaling approach by calibrating and validating bed roughness at 1:10, 1:20, and 1:30 scales and assessing the resulting model performance. A field-calibrated prototype model is first developed and then downscaled to these three ratios. Each scaled model undergoes a rigorous calibration and validation phase. The 1:10 model serves as the main benchmark for deriving a new empirical scaling relationship for Manning's n, which is then tested on the independent 1:20 and 1:30 models to assess its transferability under different geometric constraints. The study also provides a comparative assessment of roughness scaling behavior under identical hydraulic forcing. The analysis focuses on relative model behavior and parameter trends rather than absolute predictive accuracy. The resulting insights offer practical guidance for engineers and water resources managers who rely on downscaled numerical models to analyze complex river systems where full-scale data are limited.

2 Material and Method

The methodological workflow proceeds from field data integration to multi-scale numerical validation. An initial high-resolution bathymetric survey creates a calibrated 2DH hydrodynamic prototype model for all subsequent comparisons. After downscaling, this prototype is 1:10, 1:20, and 1:30. The 1:10 scale model is used to derive empirical scaling relationships for Manning's n, which are validated using the 1:20 and 1:30 scale models.

3 Study Area and Prototype Data

The study reach is located on the Nile River near the Assiut Power Plant, approximately 3 km downstream of the Assiut Barrage, as shown in Fig. 1a. The hydrodynamic regime in this 8 km stretch is primarily governed by two major islands: Bani Murr and Walidia. Bani Murr Island begins immediately downstream of the barrage, splitting the river into a primary left branch (carrying approximately 58% of the total discharge) and a narrower right branch (carrying 42%) (HRI 2016). Walidia Island is situated a further 530 m downstream, adjacent to the 500 m shoreline frontage of the power plant.

Field data for model development and calibration were derived from a comprehensive survey conducted by the Hydraulic Research Institute (HRI). This survey included GPS-based topographic mapping and bathymetric soundings at 50 m intervals. Hydrodynamic boundary conditions and calibration benchmarks were established via Acoustic Doppler Current Profiler (ADCP) measurements at five strategic cross-sections (CS1–CS5), as shown in Fig. 1b.

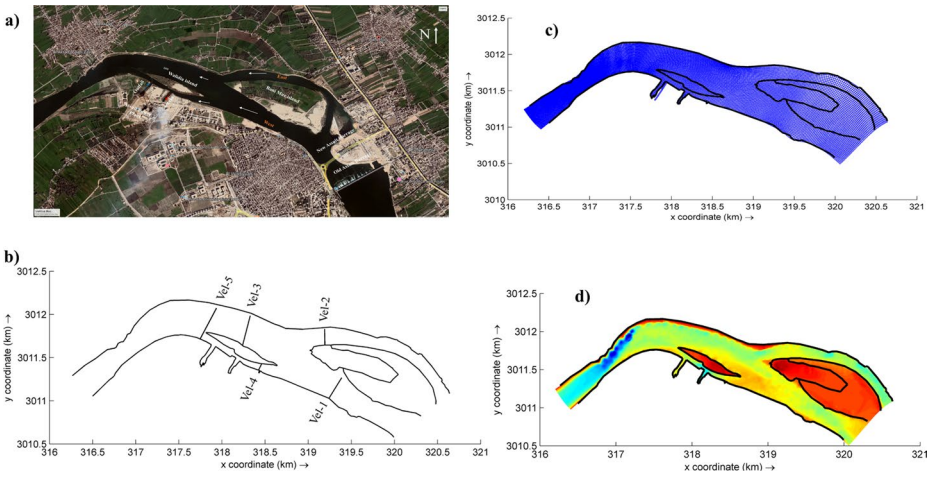

Fig. 1 Study area and model setup. (**a**) Satellite image of Nile River at Assiut. (**b**) Domain schematic with validation cross-sections CS1–CS5. (**c**) Curvilinear grid. (**d**) Interpolated bathymetry

3.1 Numerical Model Setup

A two-dimensional (2DH) numerical model was developed using the Delft3D-FLOW module to simulate depth-averaged flow patterns. The computational domain extends 2.5 km upstream and downstream of the power plant intake, covering a total reach length of 5 km and a width of approximately 0.5 km.

3.1.1 Grid Generation and Bathymetric Mapping

In Fig. 1c, a curvilinear boundary-fitted grid was used to show the complicated island shape and shoreline details. The grid resolution was refined from 30 m in the far-field to 5 m within the immediate vicinity of the power plant intake and outfall to ensure numerical accuracy in high-gradient zones. Grid orthogonality and smoothness were maintained within standard Delft3D tolerance limits. Bathymetric data were interpolated onto the grid using a triangular interpolation method, resulting in the digital elevation model presented in Fig. 1d.

3.1.2 Boundary Conditions and Parameterization

Prototype boundaries used field data. Upstream discharge: left branch 974.6 m^3/s (58%), right branch 644 m^3/s (42%). Downstream water level: 46.62 m. Walidia plant operations were modeled as a balanced sink-source (intake and outfall: ±13.89 m^3/s).

Simulations used $\rho = 1000$ kg/m^3, $g = 9.81$ m/s^2, and horizontal eddy viscosity = 1.0 m^2/s. A 30-time-step maintained numerical stability and satisfied the Courant-Friedrichs-Lewy (CFL) condition.

3.1.3 Prototype Model Calibration

The primary goal of calibrating the hydrodynamic model was to accurately reproduce measured water levels and discharge distribution (Yossef et al. 2018). The model was fine-tuned by adjusting the Manning roughness coefficient between 0.018 and 0.023 to achieve optimal agreement between computed and measured water levels, flow velocities, and water surface slope across the five cross-sections (CS1–CS5) shown in Fig. 1b.

3.2 Scaling Approach

3.2.1 Scaling Theory and Similarity Criteria

This study employs an undistorted Froude-based downscaling approach to develop three hydrodynamic models at scales of 1:10, 1:20, and 1:30. Froude similarity ensures dynamic similarity by matching inertial and gravitational forces between model and prototype. The governing scaling ratios derived from Froude similarity are summarized in Table 1 .

In natural rivers, flow occurs at high Reynolds numbers within the fully turbulent regime (Milne et al. 2021). Maintaining a high enough Reynolds number to ensure turbulent flow is very important in scaled models, even if it's not possible to match the exact prototype Reynolds number (Gustenyov et al. 2022). Once both model and prototype flows are fully turbulent, viscous effects become negligible, and Froude similarity governs flow dynamics. To minimize viscous scale effects, the Reynolds number for each scaled model was calculated during simulations and verified to exceed the established practical minimum of 2000 (Chow 1959).

Because the model is two-dimensional, vertical boundary layer processes are parameterized rather than explicitly resolved. The horizontal eddy viscosity coefficient was reduced in scaled models—from 1.0 m^2/s in the prototype to 0.1, 0.05, and 0.03 m^2/s at 1:10, 1:20, and 1:30 scales, respectively. As model scale decreases, the maximum possible eddy size is geometrically limited by reduced water depth and channel width. This viscosity reduction ensures that turbulent mixing length scales appropriately with model dimensions, maintaining the dynamic similarity of lateral momentum transfer despite the unavoidable Reynolds number mismatch inherent in Froude-scaled models.

3.2.2 Scaled Model Development

The downscaling process produced three models adhering to strict criteria for mesh orthogonality and smoothness within the Delft3D framework. A complete summary of theoretical scaling ratios, physical model dimensions, and grid characteristics is provided in Table 1. The numerical models were downscaled in both spatial extent and resolution using their respective scaling factors. The resulting computational meshes are shown in Fig. 2 **(left column: a**, **c**, **e)**. To maintain topographic consistency, prototype bathymetry was mapped onto these grids via an interpolation procedure, as visualized in Fig. 2 **(right column: b**, **d**, **f)**. This ensures that the morphological features of the riverbed are consistently represented across all numerical scales.

The hydrodynamic boundary conditions for the three scaled models, including upstream discharge distribution and downstream water level controls, were calculated based on the

Table 1 Consolidated scaling ratios, model specifications, and boundary conditions

Parameters	Scale 1:10	Scale 1:20	Scale 1:30	Rationale/ Type
(Prototype/model) Scaling Ratio				
Length scale ratio $\lambda = n_h$	10	20	30	Geo-metric similarity
Velocity scale ratio $n_v = (\lambda)^{0.5}$	3.16	4.47	5.47	Froude similarity
Time scale $n_t = (\lambda)^{0.5}$	3.16	4.47	5.47	Froude similarity
Discharge scale ratio $n_Q = (\lambda)^{2.5}$	316.23	1788.85	4929.5	Froude similarity
Model Geometry & Grid				
Length along the Nile (m)	450	250	150	Domain scaling
Reach Width (m)	130	65	45	Domain scaling
Cell Size Range (m)	0.5–2.0	0.5–1.5	0.3–1.0	Mesh Quality
Boundary Condition				
Upstream – Right branch Q (m^3/s)	2.04	0.36	0.13064	Inflow
Upstream – Left branch Q (m^3/s)	3.08	0.544	0.1977	Inflow
Downstream water level (m)	4.662	2.331	1.554	outflow
Walidia intake Q (m^3/s)	-0.02196	-0.0077	-0.00141	Sink
Walidia outfall Q (m^3/s)	0.02196	0.0077	0.00141	Source

derived scaling ratios and are detailed in the lower section of Table 1. Model simulations utilized standard freshwater parameters: uniform water density of 1000 kg/m³ and gravitational acceleration of 9.80 m/s². The computational time step ($\Delta_{t\ model}$l) was also adjusted according to the Froude number relationship $\Delta_{tmodel} = \Delta_{t\ prototype} \cdot (\lambda)^{0.5}$. This ensured that the Courant-Friedrichs-Lewy (CFL) condition for numerical stability was satisfied at all scales.

3.3 Derivation of Scaling Relationships

The primary objective of this study is to compare roughness scaling behavior across multiple geometric scales under identical hydraulic forcing. Therefore, conclusions are based on relative model behavior rather than absolute predictive accuracy. The prototype model was calibrated using available field observations. In contrast, the reduced-scale models were evaluated relative to the prototype results—the only available reference, since measurements at smaller scales do not physically exist in nature. This approach is consistent with

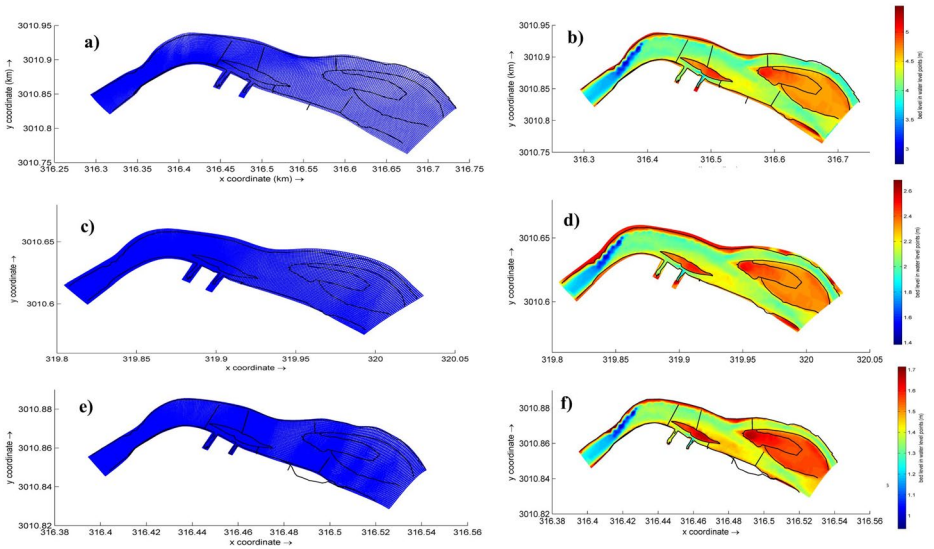

Fig. 2 Scaled model grids and bathymetry. Left column (**a**, **c**, **e**): computational grids at 1:10, 1:20, and 1:30 scales. Right column (**b**, **d**, **f**): corresponding bed levels

standard practice in scaling studies, where the validated prototype serves as the benchmark for assessing scaled model performance. The initial phase of parameter derivation focused on the 1:10 scale model. An iterative calibration process was performed to determine the optimal Manning's n that best reproduced the water levels and velocities simulated by the calibrated prototype model. The derived empirical scaling relationships were then validated using the 1:20 and 1:30 scale models.

3.3.1 Calibration of Scaled Models (Utilizing 1:10 Scale Model)

The 1:10 scale model is used as the primary reference for fine-tuning the Manning's n value. A comprehensive sensitivity analysis was conducted during this stage; this calibrated Manning's n is then used to establish correlations between the prototype and scaled parameters. The hydrodynamic outputs, specifically water levels, from each scaled simulation were quantitatively compared against the baseline prototype model at the five cross-sections shown Fig. 2b. The scenario yielding the optimal fit for water levels, determined by the lowest Root Mean Square Error (RMSE) and highest correlation coefficient (R), was then selected for subsequent velocity calibration. Table 2 presents five scenarios with different Manning's n values.

3.3.2 Validation of Scaling Relationships (Utilizing 1:20 and 1:30 Scale Models)

For the validation phase at each scale ($\lambda = 20$ and $\lambda = 30$), an identical set of five calibration scenarios, defined by a range of Manning's (n) values detailed in Table 2 was executed. The length scale ratio (L_r) for each model was defined as $L_r = 1/\lambda$, corresponding to $L_r \approx 0.05$ for the 1:20 model and $L_r \approx 0.033$ for the 1:30 model. Hydrodynamic outputs from each scaled simulation were quantitatively compared against the baseline prototype model results at the

Table 2 Summary of tested roughness scenarios, including baseline, reduction, and increment percentages for the three downscaled numerical models

Scale	Scenario	Roughness (high value)	Roughness (Low value)	Rationale
1:10	S1-10 A	0.023 (Prototype)	0.018	Baseline
	S1-10B	0.020	0.016	13% reduction
	S1-10 C	0.017	0.014	26% reduction
	S1-10D	**0.015**	**0.012**	**35% reduction**
	S1-10E	0.028	0.02	22% increment
1:20	S1-20 A	0.023 (Prototype)	0.018	Baseline
	S1-20B	0.018	0.014	22% reduction
	S1-20 C	0.016	0.013	30% reduction
	S1-20D	**0.014**	**0.011**	**39% reduction**
	S1-20E	0.028	0.02	22% increment
1:30	S1-30 A	0.023(Prototype)	0.018	Baseline
	S1-30B	0.015	0.012	34% reduction
	S1-30 C	**0.013**	**0.01**	**43% reduction**
	S1-30D	0.011	0.009	48% reduction
	S1-30E	0.025	0.019	8% increment

five consistent validation cross-sections (CS1–CS5). The scenario yielding the optimal fit for water levels (lowest RMSE, highest R) was selected for subsequent velocity calibration. This process ensured that the final validated model for each scale accurately reproduced both the water surface elevation and flow velocity fields of the prototype.

3.4 Statistical Metrics and Evaluation Methodology

The performance of each calibration scenario was quantitatively assessed by comparing simulated values (S_i) against prototype values (P_i) at consistent locations. Two complementary metrics were employed:

Root Mean Square Error (RMSE) Measures average error magnitude; values closer to zero indicate a better fit.

$$RMSE = \sqrt{\frac{1}{N}\sum_{i=1}^{N}(si - p_i)^2} \tag{1}$$

Pearson Correlation Coefficient (R) Measures linear agreement between datasets; values range from 0 to 1, with values close to 1 indicating high correlation (Williams and Esteves 2017).

$$R = \frac{N\sum_{i=1}^{N}(S_i P_i) - \left(\sum_{i=1}^{N} S_i\right)\left(\sum_{i=1}^{N} P_i\right)}{\sqrt{\left[N\sum_{i=1}^{N} S_i^2 - \left(\sum_{i=1}^{N} Si\right)^2\right]\left[N\sum_{i=1}^{N} P_i^2 - \left(\sum_{i=1}^{N} P_i\right)^2\right]}} \quad (4)$$

Roughness values were iteratively adjusted until minimum RMSE was achieved, with scatter plots and correlation statistics providing additional validation of agreement between prototype and scaled model results.

4 Results and Analysis

This section presents the results of the hydrodynamic model calibration for the prototype model and the three scaled models (1:10, 1:20, and 1:30) and discusses the implications of these findings. The results consistently demonstrated that a significant reduction in Manning's roughness coefficient from the prototype value was necessary to achieve an accurate reproduction of water levels in the scaled models.

4.1 Prototype Model Results

The selected cross sections, as previously shown in Fig. 1b were used as reference points for calibration. The calibration results for both water levels and flow velocities are presented in Fig. 3. The calibrated prototype model (Manning's $n = 0.023$) achieves excellent agreement with field observations. Water level predictions show a mean absolute error of ±0.03 m, with all computed values within 0.05 m of field measurements. Velocity comparisons yield correlation coefficients exceeding 0.95 at all validation sections, with a root mean square

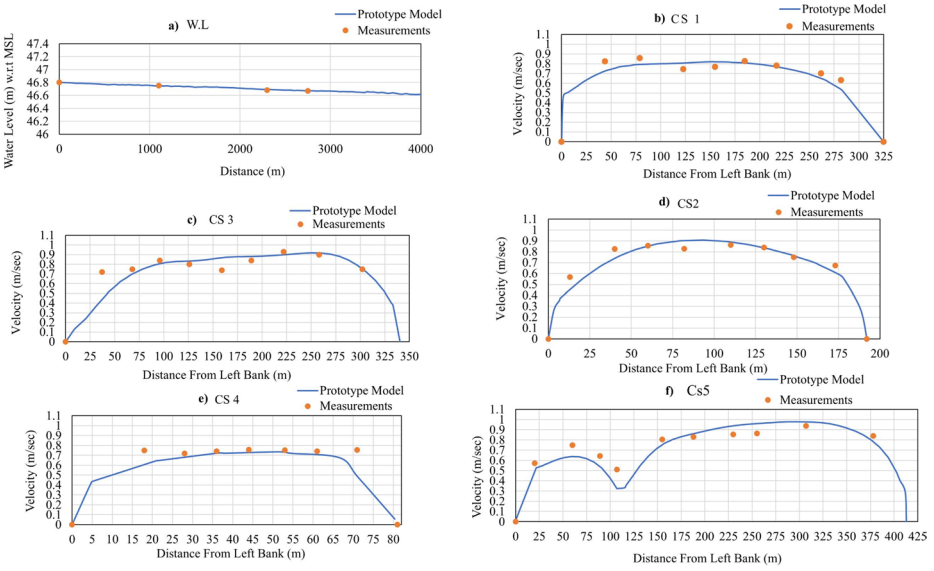

Fig. 3 Prototype model calibration. (**a**) Measured vs. computed water levels. (**b**–**f**) Velocity profiles at CS1–CS5: ADCP measurements (markers) and model results (lines)

error of 0.07 m/s. This thoroughly validated prototype serves as the essential baseline for all subsequent downscaling investigations.

4.2 Scaled Model Results

This section presents the results of the hydrodynamic model calibration for the three scaled models (1:10, 1:20, and 1:30) and discusses the implications of these findings. The results consistently demonstrated that a significant reduction in Manning's roughness coefficient from the prototype value was necessary to achieve an accurate reproduction of water levels in the scaled models.

4.2.1 Water Level Calibration Results

Figure 4 presents comprehensive calibration results comparing prototype and scaled models, after multiplying by the scale, across all three scales. The figure integrates water level profiles for multiple scenarios at 1:10, 1:20, and 1:30 scales.

Water level calibration demonstrates that significant roughness reduction is required at smaller scales. At 1:10 scale, scenario S1-10D (n=0.015) achieves the lowest RMSE of 0.0002 m with R=0.989, representing a 35% reduction from prototype roughness. The unscaled scenario (S1-10 A, n=0.023) yields the highest RMSE of 0.011 m. At 1:20 scale, S1-20D (n=0.014) achieves RMSE of 0.0003 m and R=0.992 (39% reduction). At 1:30 scale, S1-30 C (n=0.013) achieves RMSE of 0.0004 m and R=0.991 (43% reduction). Optimal values decrease systematically: 0.015 (1:10) → 0.014 (1:20) → 0.013 (1:30). Unscaled scenarios produce errors 25–50× higher than optimal configurations, confirming that prototype roughness cannot be applied directly to scaled models.

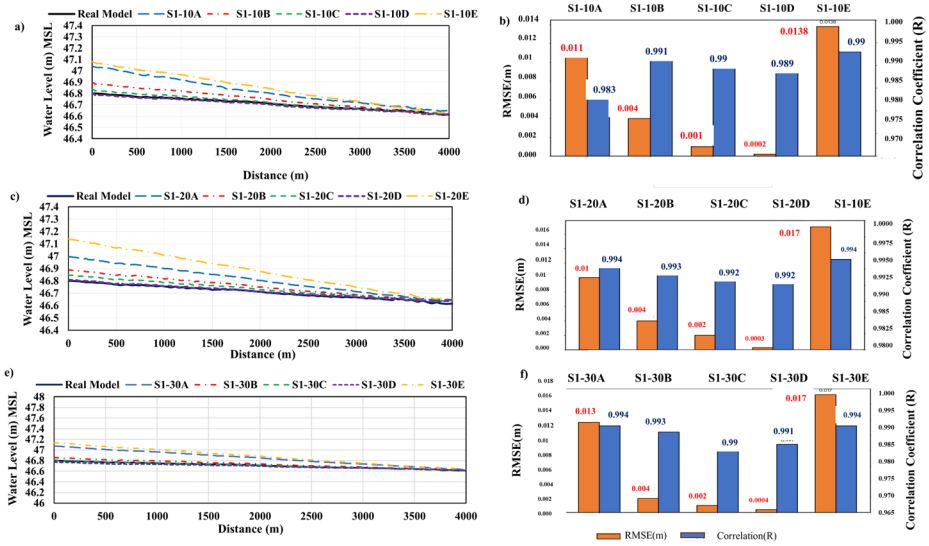

Fig. 4 Water level calibration at all scales. (**a**, **c**, **e**) Longitudinal profiles at 1:10, 1:20, and 1:30 scales comparing five scenarios (**A**–**E**) to the prototype. (**b**, **d**, **f**) Corresponding RMSE and R values

4.2.2 Velocity Calibration Results for the Optimal Scenarios

Following the water level calibration, velocity fields were evaluated for the optimal scenarios at each scale: S1-10D (1:10, $n=0.015$), S1-20D (1:20, $n=0.014$), and S1-30 C (1:30, $n=0.013$). Figure 5 presents velocity profiles at cross-sections CS1-CS5 for all three scales, with performance metrics embedded in each panel.

The results demonstrate strong agreement between prototype and scaled models, with 13 of 15 cross-sections achieving $R>0.90$. Cross-Sect. 3 shows near-perfect performance across all scales ($R\geq0.98$, RMSE$\leq$0.009 m/s). Cross-Sect. 4 exhibits elevated but scale-consistent errors (RMSE 0.09–0.12 m/s), indicating limitations of 2D modeling in complex geometry rather than scaling methodology failure. The 1:20 scale shows the most consistent overall performance (mean $R=0.945$, mean RMSE$=$0.025 m/s).

4.2.3 Sensitivity Analysis: Baseline Roughness Selection

The robustness of the numerical framework was verified by perturbing the optimal n values by ±10% and ±20% (Fig. 6d). As shown in Fig. 6a–b, both the prototype and scaled model ($\lambda=20$) exhibited near-identical hydrodynamic responses. A 20% increase in roughness raised water levels by ~0.023 m, while velocity showed the expected inverse relationship.

The convergence of mean deviations in Fig. 6c explicitly validates the preservation of hydraulic similitude. The overlap between prototype trends (lines) and scaled markers (circles/squares) proves that the 2DH domain maintains physical sensitivity across scales, confirming that the derived roughness represents a stable hydraulic equilibrium.

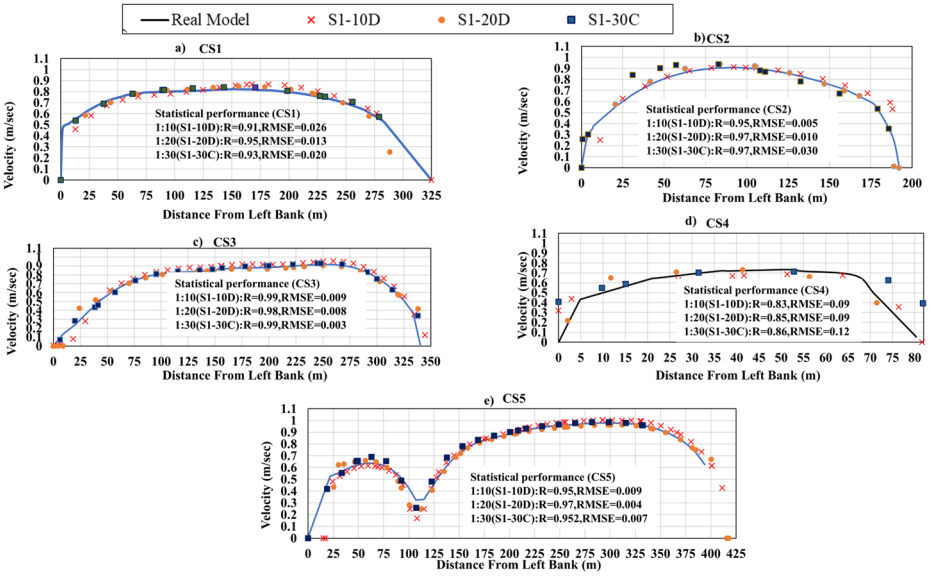

Fig. 5 Velocity validation for optimal scenarios at 1:10 (S1-10D), 1:20 (S1-20D), and 1:30 (S1-30 C)

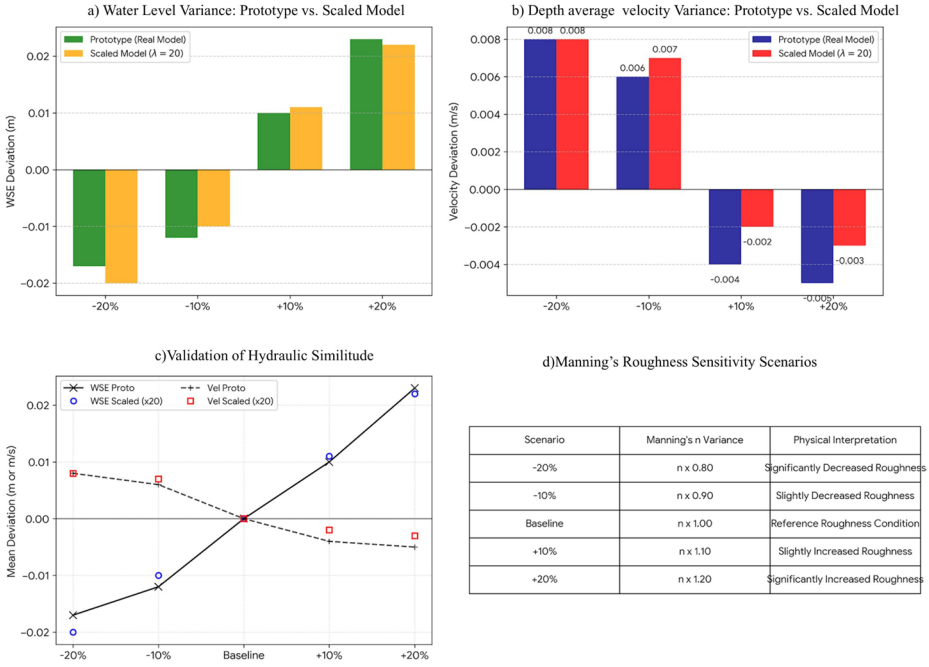

Scenario	Manning's n Variance	Physical Interpretation
-20%	n x 0.80	Significantly Decreased Roughness
-10%	n x 0.90	Slightly Decreased Roughness
Baseline	n x 1.00	Reference Roughness Condition
+10%	n x 1.10	Slightly Increased Roughness
+20%	n x 1.20	Significantly Increased Roughness

Fig. 6 Sensitivity analysis (±10%, ±20% roughness perturbations). (**a**) Water level response. (**b**) Velocity response. (**c**) Correlation of mean deviations between prototype and scaled model (λ=20). (**d**) Scenario summary

4.3 Empirical Equation for Scaling Manning's Roughness

The experimental data collected during the calibration process (Scenarios A–E) indicated a slightly more pronounced reduction requirement. The optimal roughness was found to be ns =0.015 for the 1:10 scale model (λ=10), ns=0.014 for the 1:20 scale model (λ=20), and ns =0.013 for the 1:30 scale model (λ=30). The prototype roughness is n_p=*0.023*. By applying a power-law $n_s=n_p \cdot \lambda^x$ to these calibration points, the best-fit exponent was determined to be **-0.18**, as expressed in Eq. (3).

$$n_s = n_p \cdot \lambda^{-0.18} \tag{3}$$

Where:

- ns is Manning's roughness coefficient for the scaled model.
- np is the Manning's roughness coefficient for the prototype model.
- λ is the length scale ratio (e.g., 10 for a 1:10 scale model, 20 for a 1:20 model).

The calibration data from Scale 1:10 was used to solve the Exponent (x):

$$0.015 = 0.023 \cdot 10^{x}$$

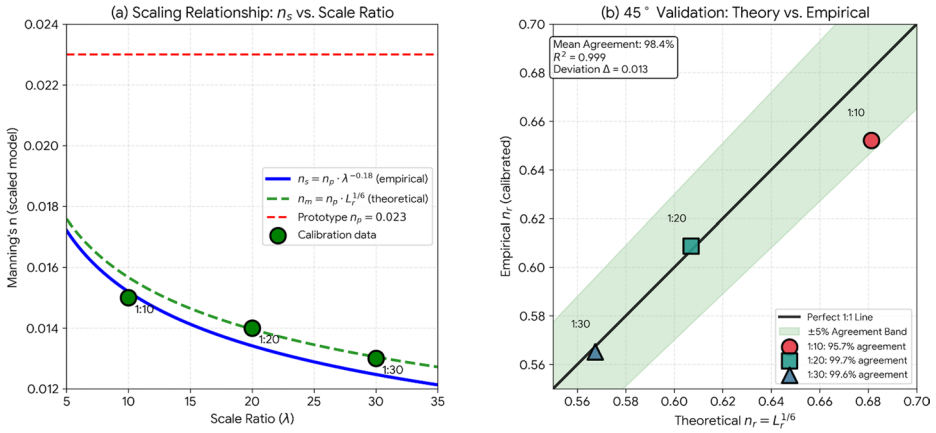

Fig. 7 Empirical scaling relationship. (**a**) Calibrated n values vs. theoretical Froude scaling (dashed line) and proposed equation ns=np·λ^(-0.18) (solid line). (b) 45° validation plot: theoretical vs. empirical roughness ratios

By using the log function, we can calculate the value: x≈−0.185.

To validate and refine the value of x, we use the calibration data from Scale 1:20 and Scale 1:30.

- For λ=20: x= ($\log_{20} = \frac{0.014}{0.023}$)≈−0.18.
- For λ=30: x=($\log_{30} = \frac{0.013}{0.023}$)≈−0.18.

4.4 Theoretical Validation and Comparative Scaling

The empirical scaling relationship derived in Eq. (3) was benchmarked against the classical scaling law discussed in the Introduction. As previously noted, while maintaining dynamic similitude in free-surface flows requires Froude similarity ($Fr_m = Fr_p$), the structural form of the Manning equation dictates a specific theoretical scaling ratio: $n_r = L_r^{1/6}$ or $ns = np.\lambda^{-0.167}$.

This relationship, often cited as the unique mathematical consequence of satisfying Froude similarity within a friction-based framework, serves as the standard theoretical limit. Figure 7 illustrates the alignment between our calibrated Manning's n values and this theoretical curve.

The results show a mean agreement of **98.1%** across all scales, with the 1:20 scale achieving the highest convergence at **99.5%**. The small deviation Δ=0.013 between theoretical and empirical exponents is quantified here and interpreted physically in the Discussion.

5 Discussion

The systematic reduction in optimal Manning's n with decreasing scale—0.015 (1:10) → 0.014 (1:20) → 0.013 (1:30)—confirms that prototype roughness cannot be applied directly to scaled models. The derived relationship $n_s = n_p \cdot \lambda^{-0.18}$ provides a robust predictive tool, with the exponent independently verified at each scale. Unscaled roughness produces

water level errors 25–50× higher than optimal scenarios, underscoring the necessity of scale-dependent adjustment.

The 98.1% agreement between empirical results and theoretical Froude scaling ($L_r^{1/6}$ exponent − 0.167) confirms that calibrated values are grounded in fundamental hydraulic theory.

The small deviation Δ = 0.013 between theoretical (-0.167) and empirical (-0.18) exponents is not an error but the quantitative signature of unresolved physical processes:

- **Boundary layer growth**: Relative boundary layer thickness increases effective bed friction at smaller scales. In the 2D depth-averaged framework, vertical processes are parameterized, with this effect absorbed into calibrated Manning's n.
- **Turbulence distortion**: As detailed in Sect. 2.3, reduced eddy viscosity—from 1.0 in the prototype to 0.1, 0.05, and 0.03 at 1:10, 1:20, and 1:30 scales, respectively—accounts for physical constraints on turbulent eddy size in smaller domains.

The systematic reduction in effective roughness within narrow Sects. (15–23% across all scales) proves that turbulence distortion depends on channel geometry. This confirms that the viscosity adjustments described in Sect. 2.3 are correct—the calibrated parameters capture the net effect of small-scale turbulence, allowing scaled models to match prototype behavior even though the 2D model cannot simulate every turbulent eddy.

The scale effect factor $f_{scale} = n_{cal}/n_{theor}$ varies systematically across scales: 0.957 at 1:10, 1.005 at 1:20, and 1.009 at 1:30. This change shows that there are two different physical processes at work, with a clear crossover at the 1:20 scale, where the effects of boundary layer growth and turbulence distortion mostly cancel each other out. This explains the exceptional 99.5% theoretical agreement, lowest water level RMSE (0.0003 m), and most consistent velocity performance (mean $R = 0.945$) observed at 1:20, identifying it as the optimal scale where scale effects minimize. Scales smaller than 1:30 may encounter increasing boundary layer distortion; scales larger than 1:10 may require compensation for turbulence-dominated effects.

Cross-Sect. 3 demonstrates near-perfect velocity reproduction ($R \geq 0.98$, RMSE ≤ 0.009 m/s) in well-behaved reaches, confirming methodology effectiveness where 2D assumptions hold. Cross-Sect. 4 exhibits elevated but scale-consistent errors (RMSE 0.09–0.12 m/s) across all scales. Critically, these errors are systematic rather than scale-dependent—the magnitude remains constant regardless of scale, indicating 2D model limitations in complex geometry rather than scaling methodology failure. The scaling relationship itself remains valid; users should anticipate higher uncertainty in geometrically complex regions where secondary currents and three-dimensional flow structures develop.

Sensitivity analysis confirms robustness: ±20% perturbations around optimal values produce symmetric response patterns, and all three scales exhibit identical sensitivity to roughness variations (deviations < 0.003 m for water levels and < 0.002 m/s for velocities). This confirms preserved dynamic similarity across the tested range.

The scaling law $n_s = n_p \cdot \lambda^{-0.18}$ provides a physics-based first estimate, eliminating trial-and-error calibration. The 1:20 scale is recommended for optimal accuracy. Validation applies to:

- Large-scale alluvial rivers with subcritical flow (Fr < 1).

- Undistorted geometric models (equal horizontal/vertical scales).
- Prismatic to moderately irregular channels at 1:10–1:30 scales.
- Fully turbulent flow in 2D depth-averaged frameworks.

While the specific exponent may vary for different river topologies (e.g., mountain streams, vegetated channels), the methodological framework is globally portable. Extension to sediment-transporting flows requires additional morphological scaling constraints beyond hydrodynamic similarity.

6 Conclusion

This research provides a comprehensive experimental validation of the scale dependency of Manning's roughness coefficient (n) using a high-fidelity 2DH numerical framework. It applies classical roughness scaling $\left(n_r = L_r^{1/6}\right)$ within complex, modern depth-averaged simulations, a topic that has remained largely unquantified. Through a rigorous cross-scale analysis (1:10, 1:20, and 1:30) in Delft3D, the study achieves a mean agreement of 98.1% with the theoretical law.

The principal novelty of this work lies in identifying a clear 'quantitative signature' of unresolved physical processes. By isolating a systematic deviation $(\Delta = 0.013)$ between the theoretical exponent -0.167 and the empirically derived exponent -0.18, the study captures the combined effects of boundary layer growth and turbulence distortion in reduced-scale models. Unlike traditional, site-specific trial-and-error approaches, it proposes a validated refinement for roughness scaling $\left(n_s = n_p \cdot \lambda^{-0.18}\right)$ that preserves theoretical rigor while offering practical predictive capability.

The results also indicate that a 1:20 scale provides the best balance between accuracy and scale effects, with very high agreement between theoretical and calibrated roughness and with low water-level and velocity errors. This gives engineers a clear, practical guideline for selecting an appropriate model scale.

The proposed workflow shifts roughness scaling from trial-and-error to a reproducible methodology applicable to similar alluvial rivers. While the findings are specific to undistorted, fully turbulent, depth-averaged flows in large alluvial rivers, they establish a quantitative baseline for extending roughness scaling to morphodynamic models, steeper channels, and more complex fluvial environments. Future work could extend this framework to sediment-transport flows, which may require additional morphological constraints, and to steeper channels or vegetated floodplains where site-specific calibration might be needed.

Author Contributions All authors contributed to the study conception, data analysis, and manuscript preparation. All authors read and approved the final manuscript.

Funding Open access funding provided by The Science, Technology & Innovation Funding Authority (STDF) in cooperation with The Egyptian Knowledge Bank (EKB). The authors received no specific funding for this work.

Data Availability The data that support the findings of this study are available on request from the corresponding author.

Declarations

Conflict of interest On behalf of all authors, the corresponding author states that there is no conflict of interest.

References

Bates PD, Quinn N, Sampson C, Smith A, Wing O, Sosa J, Savage J, Olcese G, Coxon G (2021) Combined modeling of US fluvial, pluvial, and coastal flood hazard under current and future climates. Water Resour Res 57(2):e2020WR028673. https://doi.org/10.1029/2020WR028673

Boulomytis VTG, Zuffo AC, Dalfre Filho JG (2017) Estimation and calibration of Manning's roughness coefficients for ungauged watersheds on coastal floodplains. Int J River Basin Manag 15(2):199–206. https://doi.org/10.1080/15715124.2017.1298605

Campolongo F, Cariboni J, Saltelli A (2007) An effective screening design for sensitivity analysis of large models. Environ Model Softw 22(10):1509–1518. https://doi.org/10.1016/j.envsoft.2006.10.004

Chow VT (1959) Open-Channel Hydraulics. McGraw-Hill, New York

Deltares (2022) Delft3D-FLOW simulation of multi-dimensional hydrodynamic flows and transport phenomena. Including Sediments User Manual

Devi K, Sharma A, Kumar B (2025) An experimental investigation and dimensional analysis for zonal flow prediction in compound open channels. ISH J Hydraul Eng 31(5):904–924. https://doi.org/10.1080/09715010.2025.2536810

Dottori F, Di Baldassarre G, Todini E (2013) Detailed data is welcome, but with a pinch of salt: Accuracy, precision, and uncertainty in flood inundation modeling. Water Resour Res 49(9):6079–6085. https://doi.org/10.1002/wrcr.20406

Gioia G, Bombardelli FA (2001) Scaling and similarity in rough channel flows. Phys Rev Lett 88(1):014501. https://doi.org/10.1103/PhysRevLett.88.014501

Gustenyov N, Bailey S, Egerer M, Hultmark M, Smits AJ (2022) Modeling dissipation scale distributions at high Reynolds number. In: AIAA AVIATION 2022 forum. p 3346. https://doi.org/10.2514/6.2022-3346

Hameed LK (2013) Estimating of Manning's roughness coefficient for Hilla River through calibration using HEC-RAS model. Jordan J Civ Eng 7(4):456–468.

Haroun K, Ghomri A, Besser D, Herri I (2025) ASemi-theoretical study on the effect of rough beds on the conjugate depth ratio in hydraulic jumps. Eng Technol Appl Sci Res 15(1):123–130. https://doi.org/10.48084/etasr.10754

Heller V (2011) Scale effects in physical hydraulic engineering models. J Hydraul Res 49(3):293–306. https://doi.org/10.1080/00221686.2011.578914

Horritt MS, Bates PD (2002) Evaluation of 1D and 2D numerical models for predicting river flood inundation. J Hydrol 268(1–4):87–99. https://doi.org/10.1016/S0022-1694(02)00121-X

Hydraulics Research Institute (HRI) (2016) Morphological modelling for capacity extension of Assiut Power Plant (baseline morphological modelling). National Water Research Center, Egypt

Kant C, Meena RS, Singh SK (2025) A critical appraisal on various hydrological and hydrodynamic models. Water Conserv Sci Eng 10:24. https://doi.org/10.1007/s41101-024-00328-x

Lazzarin T, Viero D (2022) Curvature-induced secondary flow in 2D depth-averaged hydro-morphodynamic models: An assessment of different approaches and key factors. Adv Water Resour 170:104355. https://doi.org/10.1016/j.advwatres.2022.104355

Milne I, Graham JMR, Coles D (2021) On the scaling of turbulence in a high Reynolds number tidal flow. J Fluid Mech 915:A58. https://doi.org/10.1017/jfm.2021.169

Morris MD (2018) Factorial sampling plans for preliminary computational experiments. Technometrics 33(2):161–174. https://doi.org/10.1080/00401706.1991.10484804

Neal J, Schumann G, Bates P (2012) A subgrid channel model for simulating river hydraulics and floodplain inundation over large and data sparse areas. Water Resour Res 48(11):W11506. https://doi.org/10.1029/2012WR012514

Rad H, Ebrahimian H, Liaghat A, Omid M, Khalaji F, Arani M (2025) Integrating image processing and machine learning for phase specific estimation of Manning roughness coefficient in furrow irrigation. Sci Rep 15:37062. https://doi.org/10.1038/s41598-025-20805-0

Saltelli A, Aleksankina K, Becker W, Fennell P, Ferretti F, Holst N, Li S, Wu Q (2019) Why so many published sensitivity analyses are false: A systematic review of sensitivity analysis practices. Environ Model Softw 114:29–39. https://doi.org/10.1016/j.envsoft.2019.01.012

Shahverdi K, Talebmorad H (2023) Automating HEC-RAS and linking with particle swarm optimizer to calibrate Manning's roughness coefficient. Water Resour Manag 37:975–993. https://doi.org/10.1007/s11269-022-03422-8

Tartandyo R, Ginting BM, Zulfan J (2024) Scale effects investigation in physical modeling of recirculating shallow flow using large eddy simulation technique. J Appl Fluid Mech 17(1):1980–1992. https://doi.org/10.47176/jafm.17.1.1980

Teng J, Jakeman AJ, Vaze J, Croke BF, Dutta D, Kim S (2017) Flood inundation modelling: A review of methods, recent advances and uncertainty analysis. Environ Model Softw 90:201–216. https://doi.org/10.1016/j.envsoft.2017.01.006

Williams JJ, Esteves LS (2017) Guidance on setup, calibration, and validation of hydrodynamic, wave, and sediment models for shelf seas and estuaries. Adv Civ Eng 2017:5251902. https://doi.org/10.1155/2017/5251902

Windt C, Davidson J, Ringwood J (2021) Numerical analysis of the hydrodynamic scaling effects for the Wavestar wave energy converter. J Fluids Struct 105:103328. https://doi.org/10.1016/j.jfluidstructs.2021.103328

Yang R, Wu S, Gao X, Wu X, Zhang C, Wang C, Zhao Y (2021) An accuracy-improved flood risk and ecological risk assessment in an interconnected river–lake system based on a copula-coupled hydrodynamic risk assessment model. J Hydrol 603:127042. https://doi.org/10.1016/j.jhydrol.2021.127042

Yossef MFM, de Jong JS, Spruyt A, Scholten M (2018) Novel approaches for large-scale two-dimensional hydrodynamic modelling of rivers. In: E3S Web of Conferences, vol 40, p 05040. https://doi.org/10.1051/e3sconf/20184005040

Yuan Y, Lozano-Durán A (2025) Dimensionless learning based on information. Nat Commun 16:9171. https://doi.org/10.1038/s41467-025-64425-8

Zafar MB, Phanikumar MS (2026) Temporal transferability of spatially derived Manning's roughness across flood regimes in the Mississippi River. J Hydrol 645:135186. https://doi.org/10.1016/j.jhydrol.2026.135186